Synchrophasing as a Noise Reduction Tool in Distributed Electric Propulsion Systems during Flight

Aryan Nikhil Thosar[1], Rudy Cepeda-Gomez[2], and Thomas F. Geyer[3]

[1]Research Associate, Department of Aeronautical Requirements and Control of Propulsion Systems, Lieberoser Straße 13a, Cottbus, Germany , aryan.thosar@dlr.de
[2]Group Leader, Department of Aeronautical Requirements and Control of Propulsion Systems, Lieberoser Straße 13a, Cottbus, Germany , rudy.cepedagomez@dlr.de
[3]Department Head, Department of Environmental Impact and Sensor Technology, Lieberoser Straße 13a, Cottbus, Germany , thomas.geyer@dlr.de
[4]Institute of Electrified Aero Engines, German Aerospace Center (DLR), Cottbus, Germany

August 21, 2026

Abstract

This paper presents an extension of an active control strategy, synchrophasing, to mitigate noise levels caused by Distributed Electric Propulsion. By dynamically computing specific phase differences between rotating propellers, destructive interference is sought at certain longitudinal locations on the fuselage, reducing noise exposure for passengers. To effectively implement synchrophasing, an Extremum-Seeking Controller strategy has been previously demonstrated to be able to minimize the noise perceived by external, on-ground microphones in an overflight case. This work focuses on the noise perceived

by microphones on the aircraft fuselage. Upon setting the measured Sound Pressure Level at particular microphone locations as a cost function, a minimization thereof is pursued using the relative phases as manipulated variables. This paper evaluates the utility of ESC for a preliminary in-flight model considering an arbitrary number of propellers on one side of the wing and a longitudinal array of microphones on the fuselage skin. The objective is that, on running the control algorithm, ESC should reduce the SPL at certain microphone locations. This reduction, added to the structure-based sound reduction, enables a quiet flight experience in electrified aircraft.

Nomenclature

D	=	Propeller Diameter, m
P_V	=	Volume Monopole component of pressure, Pa
P_D	=	Drag Dipole component of pressure, Pa
P_L	=	Lift Dipole component of pressure, Pa
P_m	=	Total pressure component, Pa
m	=	Harmonic number
ρ_0	=	Air density, $\mathrm{kg\,m^{-3}}$
c_0	=	Speed of sound, $\mathrm{m\,s^{-1}}$
B	=	Number of blades
i	=	Imaginary unit, $\sqrt{-1}$
Ω	=	Rotational speed of a propeller, $\mathrm{rad\,s^{-1}}$
y	=	Distance to a microphone from the propeller axis, m
r_{static}	=	Geometrical distance between propeller and microphone, m
r	=	Actual prop-mic distance travelled by the sound wave, m
z	=	Radial Station
M_x	=	Flight Mach number
M_T	=	Tip-rotational Mach number
M_r	=	Tip-helical Mach number $\sqrt{M_x^2 + z^2 M_T^2}$
θ	=	Directivity angle, rad
k_x and k_y	=	Dimensionless chordwise wavenumbers
t_b	=	Thickness to chord ratio
B_D	=	chord to diameter ratio
C_D	=	design drag coefficient
C_L	=	design lift coefficient
Ψ_V	=	Thickness source
Ψ_D	=	Drag source
Ψ_L	=	Lift source

X	=	Chordwise coordinate
H	=	Chordwise Thickness Distribution
f_D	=	Area-normalized chordwise drag distribution
f_L	=	Area-normalized chordwise lift distribution
t	=	Time variable
$p(t)$	=	Pressure time-series
ϕ	=	Propeller phase
J_E	=	Cost function
$\underline{u}_E$	=	Vector of synchrophase angles input to the plant
k	=	time-step
w	=	weight
$\underline{\hat{x}}$	=	Predicted derivative from EKF
$\hat{\mathbf{P}}_x$	=	Covariance matrix of states, here derivatives
$\hat{\mathbf{P}}_y$	=	Covariance matrix of measurements, here cost function changes
$\hat{y}$	=	Estimated change in the cost function
$\mathbf{F}$	=	Linearized system dynamics matrix
$\mathbf{H}$	=	Linearized measurement-to-state mapping
$\mathbf{K}$	=	Kalman Gain
$\mathbf{Q}$	=	Matrix of uncertainties in the state
$\mathbf{R}$	=	Matrix of uncertainties in the measurement
$\underline{\beta}_E$	=	Vector of perturbation amplitudes
$\underline{\omega}_E$	=	Vector of perturbation frequencies
$\underline{\alpha}$	=	Vector of integrator gains
$\underline{g}_E$	=	Vector of derivatives (same as $\underline{\hat{x}}$)
$\underline{n}$	=	Noise input

1 Introduction

Distributed Electric Propulsion (DEP) aircraft, which are usually propeller-driven, have lately gained significant attention due to the increasingly stringent emission standards established [4, 9]. Although these entail much lesser harmful greenhouse gas emissions, a major problem with propeller-driven systems is their noisy operation. To give a rough estimate, it is not uncommon to have sound levels of around 120 dB at a diameter's distance from a propeller in the radial direction [2]. Prolonged exposure to such levels would prove to be detrimental to the passengers seated inside the plane. Thus, a study of the noise emitted by rotating propellers at the fuselage boundary is necessary.

When propellers are driven at low to moderate tip-helical speeds, tonal noise is a major contributor to the Sound Pressure Level (SPL) [7]. This noise component is characterized by the Blade-Pass Frequency (BPF) and its higher harmonics. At trans- or supersonic speeds and small propeller tip-tip distances, the broadband component becomes significant, wherein the aerodynamic interactions between the blades, the formation and shedding of vortices, and turbulent effects contribute to the overall noise. The computation of noise levels is hence a complicated task, which further renders noise minimization challenging. This study narrows its scope down to the reduction of tonal noise levels, as DEP aircraft are expected to operate at subsonic Mach numbers and relatively low rotational speeds.

Some novel noise minimization techniques focus on a concept called synchrophasing [8, 10, 11], which seeks to find phase differences between the rotating propellers to enforce destructive interference in certain directions and at certain distances. Due to the highly nonlinear dynamics of the problem, with several sources of uncertainty, trying to derive an analytical method for the determination of such angles would be very complex. The Extremum Seeking Control (ESC) algorithm, thanks to its simplicity of implementation and its independence from the system model [1], proves to be a particularly well-suited control method to address this.

Previous works [10, 11] investigated the effect of synchrophasing using ESC for external noise. In both works, the interest was to reduce the noise perceived at certain locations on ground. This paper addresses noise perceived on an aircraft fuselage, further paving the way for noise reduction for passengers seated within.

The generic configuration shown in Figure 1 is considered in this work. The objective is to minimize the SPL perceived at an array of 13 different locations along the side of the fuselage on which the propellers are. The measurement locations are assumed to be uniformly spaced, covering 5 m up- and downstream of the wing. Cases with two and four propellers are studied. It is assumed that the closest propeller to the fuselage is at a distance of $2.5D$ from it, where D is the propeller diameter. The tip-to-tip distance between propellers is fixed at $2D$, giving a center-to-center distance of $3D$.

A numerical simulation tool based on Hanson's model [5] was developed to take the role of the plant. The mathematical backbone of this tool is described in Section 2. The control algorithm is presented in Section 3. Results of the simulations before and after the control action is implemented are presented in Section 4, whereas Section 5 concludes the paper with a brief discussion of the main observations.

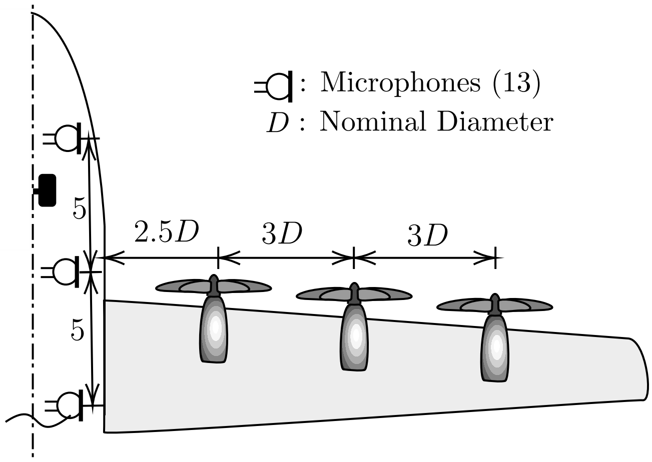

Figure 1: Example DEP Configuration under Consideration

2 Sound Field Modeling

2.1 Mathematical Model

This work uses the model introduced by Hanson [5] for the prediction of the sound generated by the propellers of the aircraft. This model postulates that the overall sound pressure at a point due to a rotating propeller is produced by a superposition of the SPL produced by different sources: the volume monopole, the lift and drag dipoles, and the stress quadrupoles. Per the definition given in [3], if the distance between source and the observer d_S is negligible when compared to the acoustic wavelength λ, the observer is said to be in the acoustic near-field of the source. Larger separations between source and observer are considered to be in the acoustic far-field. The behaviour of the sound propagation in these two regions is different and needs to be model separately. Given the distances described in the previous section, with the propeller closest to the fuselage being at a distance of more than one λ from it, this work uses far-field modeling [5]. Since the propellers have a subsonic tip-helical speed, the quadrupole sources in the sound pressure field are ignored [6]. Doppler effects in the frequencies [12] are canceled, due to the lack of relative motion between observers and sources. However, the sources and the observers have a finite distance between them, so the sound emitted by the propellers has an apparent directivity towards the microphones and the Doppler factor in the amplitude terms is retained.

The far-field model proposed by Hanson [5] has the following adapted form

$$
\begin{Bmatrix} P_{Vm} \\ P_{Dm} \\ P_{Lm} \end{Bmatrix} = -\frac{\rho_0 c_0^2 B \sin\theta \exp\left[imB\left(\frac{\Omega r}{c_0} - \frac{\pi}{2}\right)\right]}{8\pi \frac{y}{D}(1 - M_x \cos\theta)}
\times \int_0^1 M_r^2 J_{mB}\left(\frac{mBzM_T \sin\theta}{1 - M_x \cos\theta}\right) \begin{Bmatrix} k_x^2 t_b \Psi_V(k_x) \\ ik_x \frac{C_D}{2} \Psi_D(k_x) \\ -ik_y \frac{C_L}{2} \Psi_L(k_x) \end{Bmatrix} dz, \tag{1}
$$

where P_{Vm}, P_{Dm} and P_{Lm} are respectively the volume monopole, lift, and drag dipole components of the m^{th} pressure harmonic, with $\rho_0 c_0^2$ being the ambient static pressure and B the number of blades. The distance between the microphone and the propeller axis is given by y, and r is the actual distance traveled by the sound wave. The exponential function characterizes the phase lag of the sound wave reaching the microphones. The Doppler factor $\frac{1}{1-M_x \cos\theta}$ in the amplitude terms, where M_x is the flight Mach number, caters for the change in the pressure amplitudes perceived by the microphones due to the mutual motion. The Bessel function J_{mB} of the harmonic order mB describes the efficiency with which the sound propagates through the air. M_r is the section-helical/resultant Mach number of a radial point (radius normalized) z on the propeller blade due to the simultaneous forward M_x and rotational M_T Mach numbers. The directivity angle θ is the apparent angle subtended by the propeller onto the respective observer, again due to the mutual motion of the propellers and the microphones. The dimensionless chordwise wavenumbers k_x and k_y encapsulate the non-compactness of the blade along its chord, which are combined with the respective sound energy source functions Ψ. Finally, t_b is the blade thickness-to-chord ratio at the radial station z, C_D and C_L are, respectively, the design drag and lift coefficients.

The numbers k_x and k_y are expressed as

$$
k_x = \frac{2mBB_D M_T}{M_r(1 - M_x \cos\theta)}, \tag{2}
$$

$$
k_y = \frac{2mBB_D}{zM_r}\left(\frac{M_r^2 \cos\theta - M_x}{1 - M_x \cos\theta}\right), \tag{3}
$$

where B_D is the chord-diameter ratio for the particular radial station. The volume, drag, and lift sources are respectively given by

$$
\Psi_V = \int_{\frac{-1}{2}}^{\frac{1}{2}} H(X) \exp(ik_x X)\, dX, \tag{4}
$$

$$\Psi_D = \int_{\frac{-1}{2}}^{\frac{1}{2}} f_D(X) \exp(ik_x X) \, dX, \tag{5}$$

$$\Psi_L = \int_{\frac{-1}{2}}^{\frac{1}{2}} f_L(X) \exp(ik_x X) \, dX, \tag{6}$$

where $H(X)$ is the thickness distribution along a chordwise position X at a particular radial station of the blade, f_D is the area-normalized distribution of the drag forces along the chord at a particular radial station, and f_L is the area-normalized lift distribution.

After the sound is emitted from a propeller, it travels a certain distance along the flight path until it reaches the observer. Hence, the directivity angles, the distances traveled by the sound waves, and the wave phases reaching the microphones change. The apparent phase angle subtended by a propeller on a microphone due to a finite flight Mach number M_x is

$$\tan\theta = \frac{y}{x + M_x r_{\text{static}}}, \tag{7}$$

where r_{static} is the geometrical distance between the propeller and the observer and x the distance along the flight direction. The actual distance traversed by an emitted sound wave can be written as

$$r = \frac{y}{\sin\theta}. \tag{8}$$

The pressure amplitude for a particular harmonic P_{mB} is then a summation of these individual components

$$P_{mB} = P_{Vm} + P_{Dm} + P_{Lm}. \tag{9}$$

Finally, once the amplitude of a particular pressure harmonic has been determined, the time variation of the pressure is the Fourier series

$$p(t) = \sum_{m=-\infty}^{\infty} P_{mB} \exp[-imB(\Omega t - \phi)], \tag{10}$$

where ϕ is the propeller azimuthal phase, if any. For multiple propellers, the pressure time series are superimposed.

3 Extremum Seeking Control

This work follows a similar concept and implementation as proposed by [10, 11]. Figure 2 presents a block diagram of the ESC implementation. The

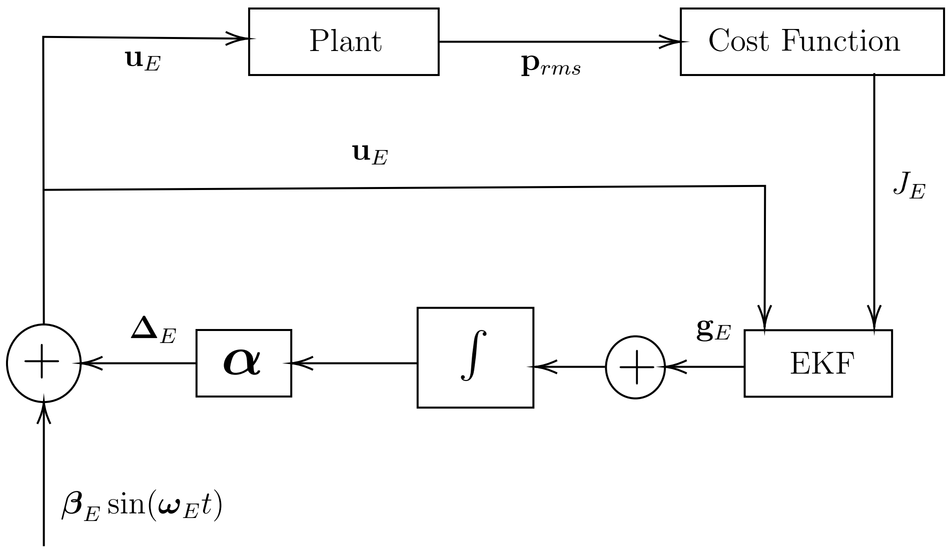

Figure 2: Block diagram of the Extremum Seeking Control Implementation [10, 11].

plant describes the propeller system, which yields certain RMS pressure levels $p_{j,rms}$ at each of the measurement locations j, given a set of synchrophase angles $\mathbf{u}_E \in R^{n_p-1}$, n_p being the number of propellers. The cost function block is user-defined and defines the quantity to be minimized. In this case, the objective function J_E is a weighted average of the sound pressure levels perceived by each observer. The Gradient Estimation block estimates the relative change of the cost function with respect to a change in the inputs to the plant $\mathbf{g}_E = \nabla_{\mathbf{u}_E} J_E$. Combined with the integrator and its gain vector $\boldsymbol{\alpha} < 0$, the output $\boldsymbol{\Delta}_E$ performs a gradient descent. A sinusoidal perturbation signal $\boldsymbol{\beta}_E \sin(\boldsymbol{\omega}_E t)$ is used to excite the system at a certain frequency, lower than the lowest characteristic frequency of the system, to ensure that the optimization method does not get trapped at a local minimum.

Once the cost function is defined, the tuning of the control algorithm is done by adjusting the perturbation signal parameters and the integral vector gain $\boldsymbol{\alpha}$. This gain and the parameter $\boldsymbol{\beta}_E$, affect the convergence characteristics of the control algorithm. If both parameters are chosen to be large, convergence might be quicker at the cost of the accuracy at the steady state. Very large $\boldsymbol{\alpha}$ can lead to a divergence in the controller output. If both the parameters are small, the system needs to run for a longer time before the extremum is reached.

Traditional ESC implementations use high-pass filters and a modulator block to estimate the gradient of the cost function [1]. This task is performed in this work by an Extended Kalman Filter (EKF).

Kalman Filters find their application in systems with uncertain models backed up by some experimental data. Based on the given model's prediction and the available measurements, a Kalman Filter makes the best possible estimate of the true state of the system, which is indeed thought to be the mean of a Gaussian distribution. Extended Kalman Filters, moreover, are used in non-linear control systems. It is assumed that not only do the state and measurement estimations follow a Gaussian-Normal distribution, but the true values do too. The estimations are denoted by a caret ($\hat{}$) on the top;

$$\underline{\hat{x}}(k) \sim \mathcal{N}_x(\underline{\hat{\mu}}_x(k), \hat{\mathbf{P}}_x(k)), \tag{11}$$

$$\underline{\hat{y}}(k) \sim \mathcal{N}_y(\underline{\hat{\mu}}_y(k), \hat{\mathbf{P}}_y(k)), \tag{12}$$

where $\underline{\hat{x}}(k)$ and $\underline{\hat{y}}(k)$ are respectively the state and the measurement estimates at a time instant k. $\underline{\hat{\mu}}(k)$ is the mean of the Gaussian distribution $\mathcal{N}$ and $\hat{\mathbf{P}}$ is the covariance matrix. Given a non-linear state-space model of a system under a state uncertainty $\underline{w}$ and a measurement uncertainty $\underline{\nu}$

$$\begin{aligned} \underline{x}(k) &= \underline{f}(\underline{x}(k-1), \underline{u}(k-1), k-1) + \underline{w}(k-1), \\ \underline{y}(k) &= \underline{h}(\underline{x}(k), k) + \underline{\nu}(k), \end{aligned} \tag{13}$$

where $\underline{f}$ is the non-linear state model and $\underline{h}$ the non-linear state-to-measurement mapping, the non-linear EKF algorithm progresses by linearizing the non-linear equations about their estimated means $\underline{\hat{\mu}}_x(k)$ and $\underline{\hat{\mu}}_y(k)$. With the starting vector $\underline{\hat{\mu}}_x(0)$ and the initial estimate of the covariance matrix of the state $\hat{\mathbf{P}}_x(0)$, the algorithm progresses as

$$\begin{aligned} \mathbf{F} &= \frac{\partial f}{\partial \underline{x}}\Big|_{\underline{x}=\underline{\hat{\mu}}_x(k-1)}, \\ \hat{\mathbf{H}} &= \frac{\partial h}{\partial \underline{x}}\Big|_{\underline{x}=\underline{\hat{\mu}}_x(k-1)}. \end{aligned} \tag{14}$$

What follows is a prediction step (denoted with arguments $(k,-)$), where the means are predicted based on the models used and the predicted covariance matrices are computed based on the linearized models added to the uncertainty matrices; for the states $\mathbf{Q}$ and for the measurements $\mathbf{R}$. This step reads

$$\begin{aligned} \underline{\hat{\mu}}_x(k,-) &= f(\underline{\hat{\mu}}_x(k-1), \underline{u}(k-1), k-1), \\ \underline{\hat{\mu}}_y(k,-) &= h(\underline{\hat{\mu}}_x(k,-), k), \\ \hat{\mathbf{P}}_x(k,-) &= \mathbf{F}\hat{\mathbf{P}}_x(k-1)\mathbf{F}^\top + \mathbf{Q}(k), \\ \hat{\mathbf{P}}_y(k,-) &= \hat{\mathbf{H}}\hat{\mathbf{P}}_x(k,-)\hat{\mathbf{H}}^\top + \mathbf{R}(k). \end{aligned} \tag{15}$$

Finally, a correction step ensues, that evaluates the estimations for the next time step k, which is written as

$$
\begin{aligned}
\mathbf{H} &= \frac{\partial h(\underline{x}, k)}{\partial \underline{x}}|_{\underline{x}=\hat{\underline{\mu}}_x(k,-)}, \\
\mathbf{K}(k) &= \hat{\mathbf{P}}_x(k,-)\mathbf{H}^\top \hat{\mathbf{P}}_y^{-1}(k,-), \\
\hat{\underline{\mu}}_x(k) &= \hat{\underline{\mu}}_x(k,-) + \mathbf{K}(k)(\underline{y}(k) - \hat{\underline{\mu}}_y(k,-)), \\
\hat{\mathbf{P}}_x(k) &= \hat{\mathbf{P}}_x(k,-) - \mathbf{K}(k)\mathbf{H}\hat{\mathbf{P}}_x(k,-).
\end{aligned}
\tag{16}
$$

For finding the derivative using EKF, the linearization steps are ignored. The changes required are

$$
\begin{aligned}
\hat{\underline{x}}(k) &\approx \frac{J_E(k) - J_E(k-1)}{\underline{u}_E(k) - \underline{u}_E(k-1)} = \hat{\underline{g}}_E, \\
\mathbf{F} &= \mathbf{I}, \\
\mathbf{H}(k) &= \operatorname{diag}(\underline{u}_E(k) - \underline{u}_E(k-1)), \\
\hat{y}(k) &= J_E(k) - J_E(k-1).
\end{aligned}
\tag{17}
$$

The derivative finding algorithm has been summarized in Algorithm 1.

4 Results

This Section compares simulation results for the system using different number of propellers. In all cases, the propellers considered are described by the parameters in Table 2 and are of the type SR-2 [2]. Microphone directivity plots, and azimuthal and meridional sound field plots are presented to understand the effects of the ESC.

The cost function J_E to be minimized by the controller is a weighted average of the root-mean-square values of the pressure signals at each observe location, represented as

$$
J_E = \sum_{k=1}^{n_m} w_k p_{rms,k}, \quad \sum_{k=1}^{n_m} w_k = 1, \tag{18}
$$

where n_m is the number of microphones. At first, uniform weights are considered: $w_k = \frac{1}{n_m}$.

Algorithm 1 Finding derivative using Extended Kalman Filter [14]

Require: Current cost function J_E(k), vector of current synchrophase angles $\underline{u}_E$(k), all under uncertainties
Ensure: Vector of derivatives $\underline{\hat{x}} \leftarrow \underline{g}_E \approx \frac{\Delta J_E}{\Delta \underline{u}_E}$

Initialise: $\underline{\hat{x}}(0,-)$, $\hat{\mathbf{P}}_x(0)$, $\underline{\hat{y}}(0)$
Set $\mathbf{Q} \leftarrow \mathbf{1}$ and $\mathbf{R}$ to be negligible
for $k \leftarrow 1$ **to** ∞ **do**
  Prediction step
  $\mathbf{F} \leftarrow \mathbf{1}$, $\mathbf{H}(k) \leftarrow \mathrm{diag}(\underline{u}_E(k) - \underline{u}_E(k-1))$
  $\underline{\hat{y}}(k,-) \leftarrow \mathbf{H}(k)\underline{\hat{x}}(k,-)$
  $\hat{y}(k) \leftarrow J_E(k) - J_E(k-1)$
  $\hat{\mathbf{P}}_x(k,-) \leftarrow \mathbf{F}\hat{\mathbf{P}}_x(k-1)\mathbf{F}^\top + \mathbf{Q}(k)$
  $\hat{\mathbf{P}}_y(k,-) \leftarrow \mathbf{H}\hat{\mathbf{P}}_x(k,-)\mathbf{H}^\top + \mathbf{R}(k)$
  Kalman Gain
  $\mathbf{K}(k) \leftarrow \hat{\mathbf{P}}_x(k,-)\mathbf{H}^\top\hat{\mathbf{P}}_y^{-1}(k,-)$
  Correction step
  $\underline{\hat{x}}(k) \leftarrow \underline{\hat{x}}(k,-) + \mathbf{K}(k)(\hat{y}(k) - \underline{\hat{y}}(k,-))$
  $\hat{\mathbf{P}}_x(k) \leftarrow \hat{\mathbf{P}}_x(k,-) - \mathbf{K}(k)\mathbf{H}\hat{\mathbf{P}}_x(k,-)$
  $\underline{\hat{x}}(k,-) \leftarrow \underline{\hat{x}}(k)$
  $\hat{\mathbf{P}}_x(k,-) \leftarrow \hat{\mathbf{P}}_x(k)$
end for

return $\underline{\hat{x}}$

Table 3: Controller Parameters in the Case with 2 Propellers

Parameter	Value
Gains $\boldsymbol{\alpha}_E$	-140
Perturbation Amplitudes $\boldsymbol{\beta}_E$	8×10^{-4}
Perturbation Frequencies $\boldsymbol{\omega}_E$	20

Table 2: Propeller and Flight parameters

Parameter	Value	Unit
Flight Mach number	0.32	-
Flight altitude	2000	m
Sound speed	332.4	$\mathrm{m\,s^{-1}}$
Number of blades	4	-
Propeller rpm	8460	$\mathrm{min^{-1}}$

4.1 Two Propellers

The first test scenario considers only two propellers on the wing. The ESC was tuned with the parametric values shown in Table 3.

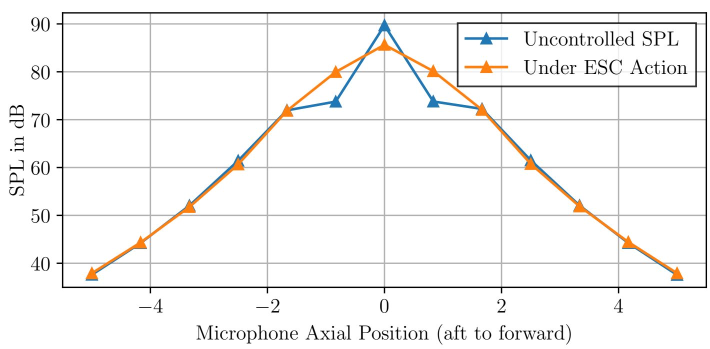

Figure 3: SPL Variation at Each Axial Position for Two Propellers.

Figure 3 compares the SPL measured at each location. With all measurements uniformly weighted, the SPL at the closest location to the propellers reduces by around 4 dB. The microphones next to the central one experience, on the contrary, an increase of almost 6.2 dB each. As has been observed in [13], synchrophasing redirects the sound energy such that pressures in certain directions are curbed at the cost of an increase in other directions.

The azimuthal directivities of the SPL for the uncontrolled and controlled cases are compared in Figures 4 and 5. In Figure 5, the origin corresponds to the position of the outermost propeller, and the fuselage is located at the rightmost vertical line of the plots. The directivity patterns 4 and 6 are plotted using the midpoint of the propellers as the center and the distance of this midpoint to the fuselage skin as the radius. These plots, together with the representation of the meridional directivity in Figures 6 and 7 illustrate how the energy is redistributed by synchrophasing. The effect of synchrophasing is to rotate and distort the sound directivity.

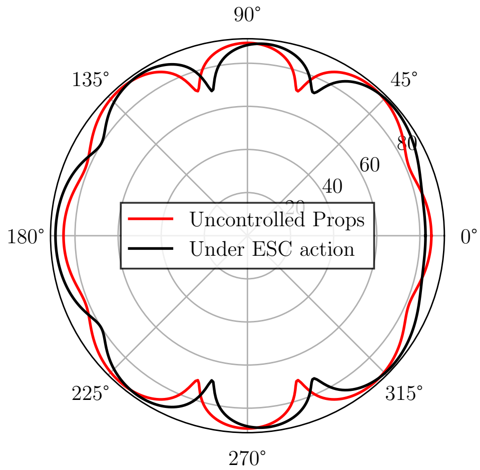

Figure 4: Azimuthal directivity pattern at radius 1.27 m.

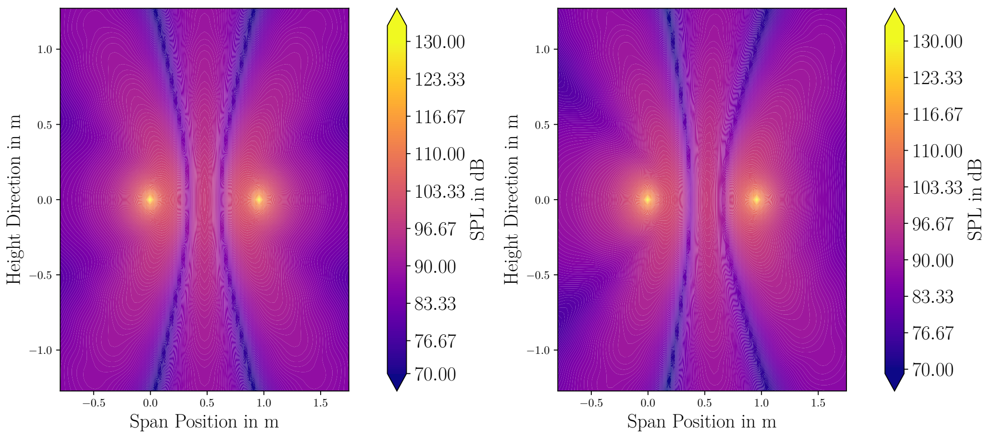

(a) Uncontrolled Propellers.

(b) Controlled Propellers.

Figure 5: Azimuthal Directivity For 2 Propellers.

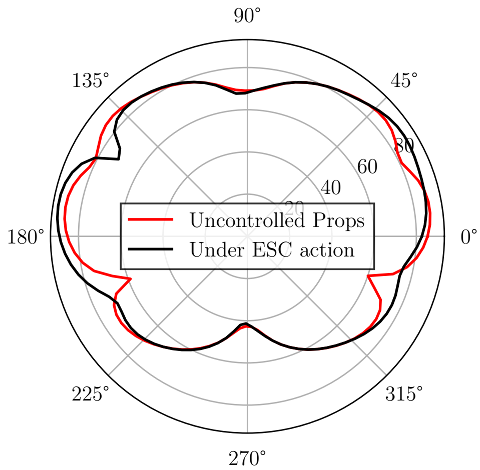

Figure 6: Meridional directivity pattern at radius 1.27 m.

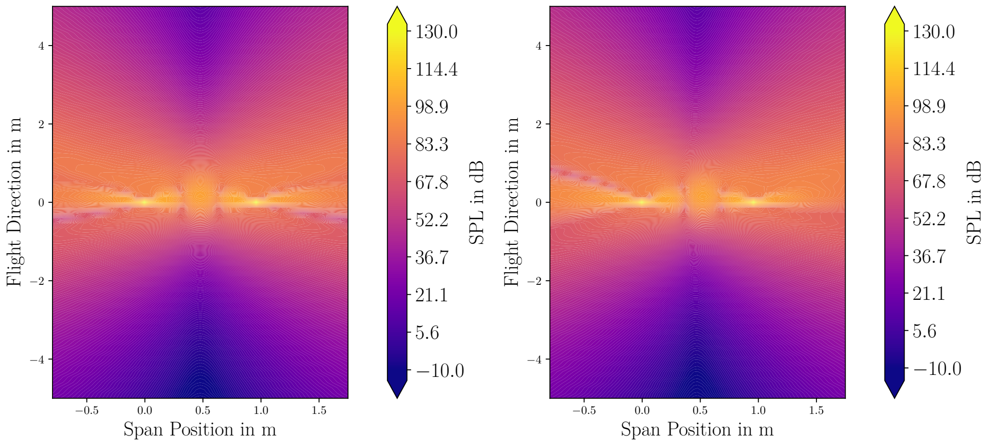

(a) Uncontrolled Propellers.

(b) Controlled Propellers.

Figure 7: Meridional Directivity For 2 Propellers.

The control action reaches steady state in about 0.2 s, as observed in Figures 8 and 9, showing, respectively, the time histories of relative phase angle between propellers and of the cost function. The phase angle commanded by the ESC fluctuates about an angle of about 12.7°. This is an expected drawback of the ESC, introduced by the perturbation function [1].

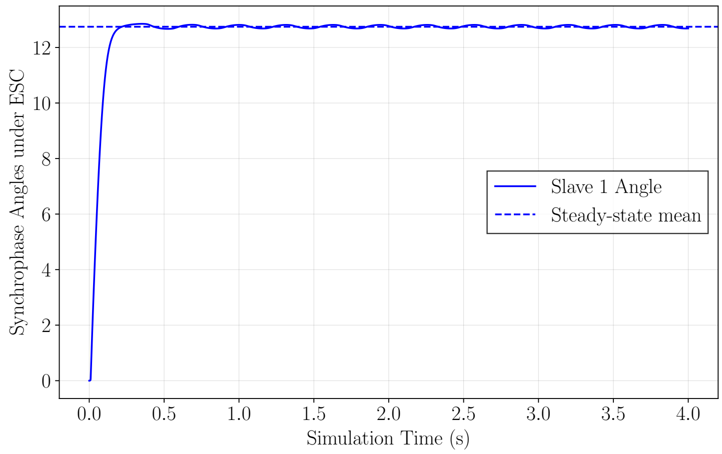

Figure 8: Time History of the Commanded Relative Phase Angle.

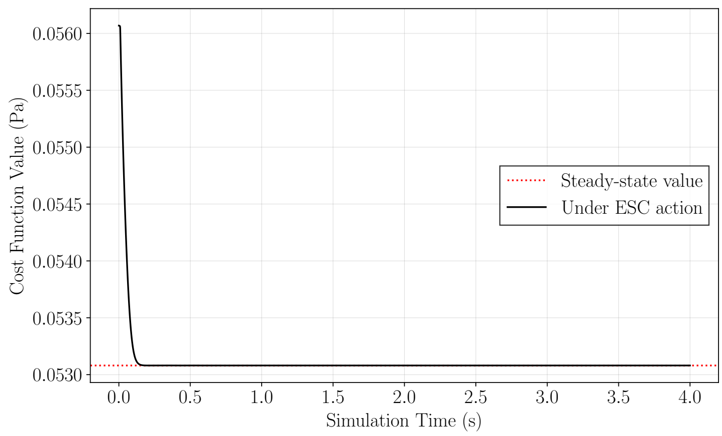

Figure 9: Time History of the Cost Function in the 2 Propeller Case.

4.2 Four Propellers

A second scenario considered four propellers. The tuning of the controller resulted in the parameters presented in Table 4. Using uniform weights for all measurements, the SPL at the central position increases after the control action, as observed in Figure 10. This is undesirable. By re-allocating the weights in the cost function, it is possible to a certain extent to flatten the SPL curve, to achieve what is observed in Figure 11. In this case, the weights were distributed as [0.012, 0.024, 0.036, 0, 0.061, 0.183, 0.366, 0.183, 0.061, 0, 0.036, 0.024, 0.012] corresponding to each microphone, numbered aft to forward. The corresponding tuning parameters can be taken from Table 5.

Although the pressure levels at microphones 6 and 8 increase after the controller action, the central microphone 7 experiences a decrease of around 4.7 dB. Hence, instead of having an abrupt change in the levels at the propeller-closest microphones, allocating larger weights at these positions renders the change smoother. For the mentioned configuration, a simultaneous decrease at the propeller-closest microphones was not possible.

Table 4: Controller tuning parameters for 4 propellers for uniform weights.

Parameter	Value
Gains $\boldsymbol{\alpha}_E$	$[-200 \ \ -220 \ \ -235]^\top$
Perturbation Amplitudes $\boldsymbol{\beta}_E$	$10^{-4} \cdot [8 \ 9 \ 7]^\top$
Perturbation Frequencies $\boldsymbol{\omega}_E$	$[20 \ 30 \ 25]^\top$

Table 5: Controller tuning parameters for 4 propellers for non-uniform weights.

Parameter	Value
Gains $\boldsymbol{\alpha}_E$	$[-92 \ \ -115 \ \ -122]^\top$
Perturbation Amplitudes $\boldsymbol{\beta}_E$	$10^{-4} \cdot [8 \ 9 \ 7]^\top$
Perturbation Frequencies $\boldsymbol{\omega}_E$	$[20 \ 30 \ 25]^\top$

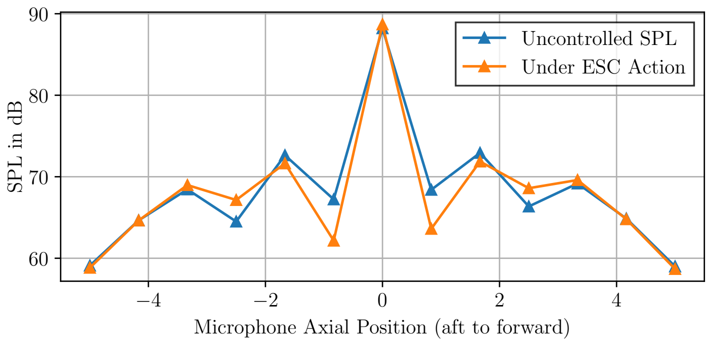

Figure 10: SPL Variation at each microphone represented by axial positions using uniform weights.

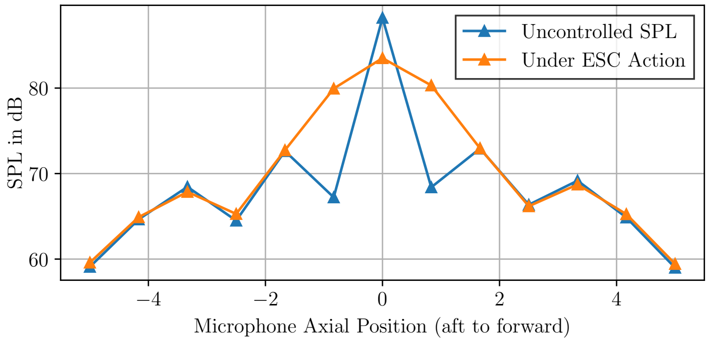

Figure 11: SPL Variation at each microphone represented by axial positions using non-uniform weights.

Substantial changes in the azimuthal and meridional directivities are respectively seen before and after the action of the ESC in Figures 12, 13 and 14, 15. The azimuthal directivity pattern in Figure 12 after the control action is yet again somewhat distorted with respect to that in the uncontrolled case.

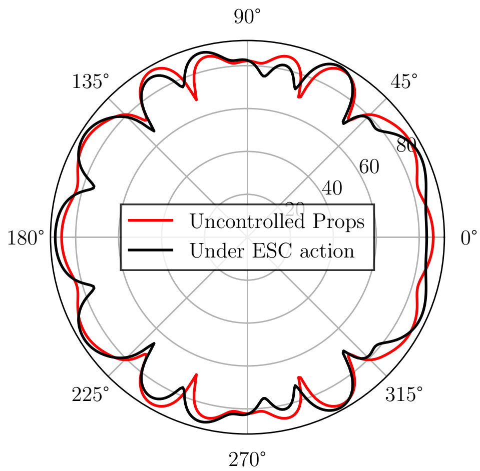

Figure 12: Azimuthal directivity pattern at radius 2.23 m using non-uniform weights.

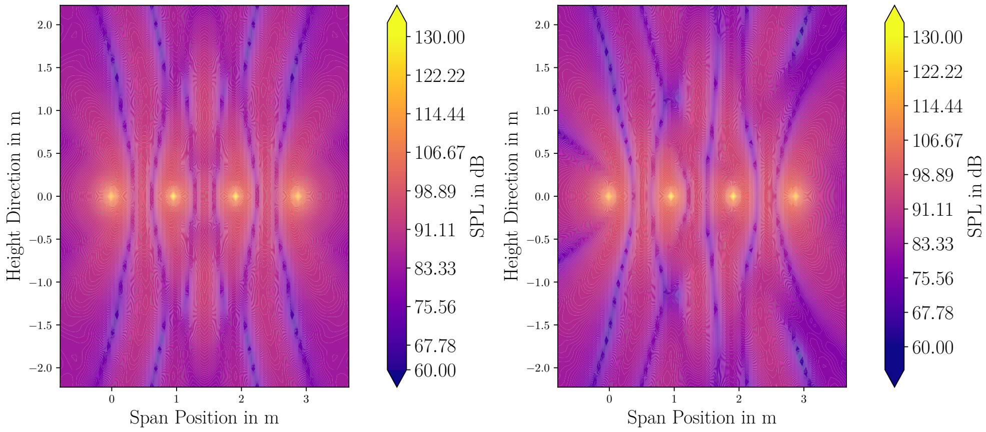

(a) Uncontrolled Propellers.

(b) Controlled Propellers.

Figure 13: Azimuthal Directivity For 4 Propellers.

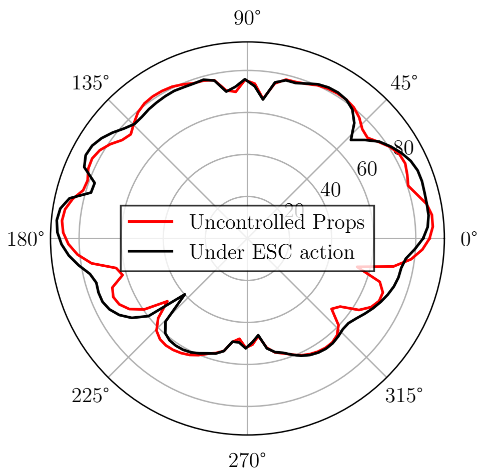

Figure 14: Meridional directivity pattern at radius 2.23 m using non-uniform weights.

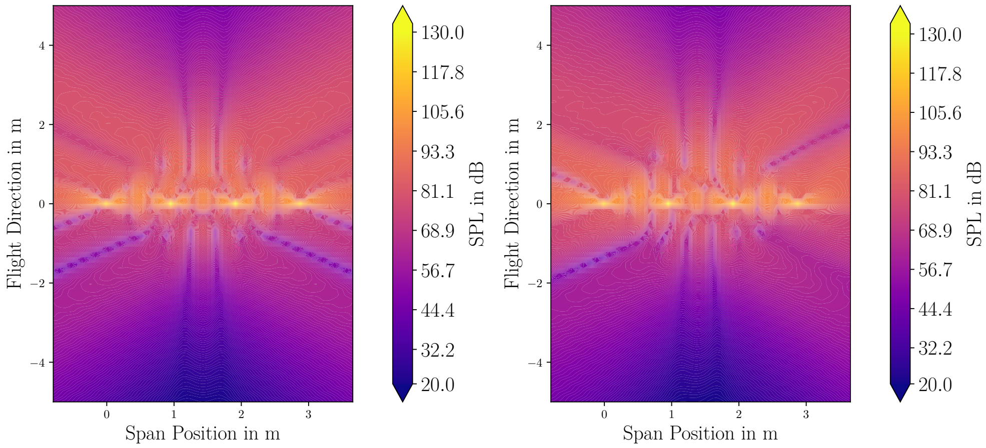

(a) Uncontrolled Propellers.

(b) Controlled Propellers.

Figure 15: Meridional Directivity For 4 Propellers.

The steady-state angles of the controller were found to have a slightly worst behavior when compared to the two-propeller case, as noticed in Figure 16. They are seen to relatively fluctuate more from their steady-state averages of 4.0°, −14.6° and −5.2°. The three synchrophase angles and the cost function in Figure 17 stabilize after three seconds of transients, indicating a slower response. Fine tuning the gains further leads to an erratic variation of the controller output. Moreover, among the two cases, the authors found this case the most challenging to tune, which could be due to an interplay between the three different synchrophase angles and the given spatial configuration. This could also imply an increased difficulty to tuning and a higher sensitivity to varying controller parameters, if the number of controlled variables increases.

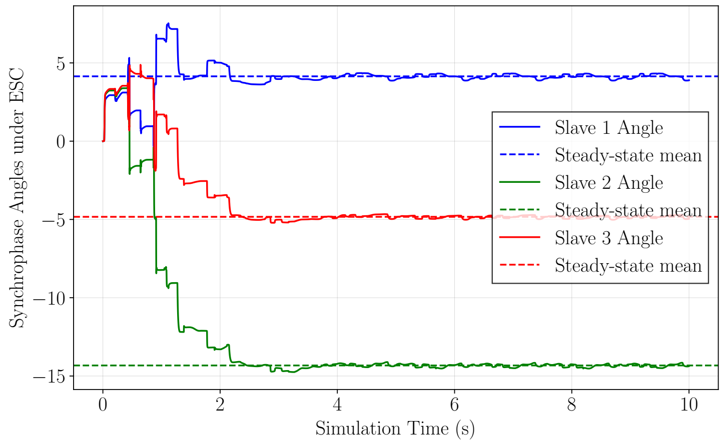

Figure 16: Time History of the Commanded Relative Phases Between Propellers using non-uniform weights.

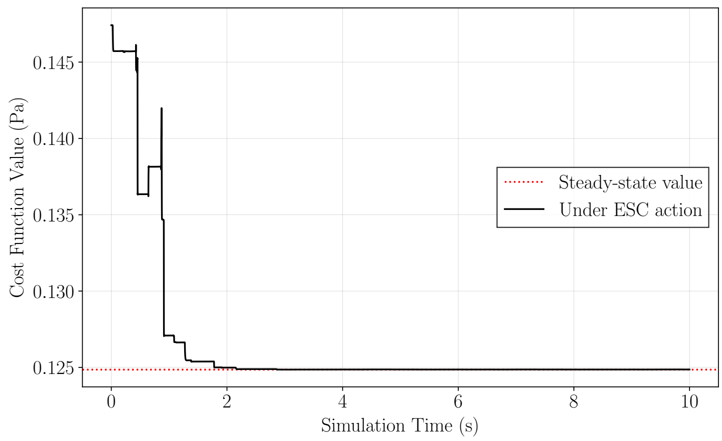

Figure 17: Time History of the Cost Function for the Case with 4 Propellers using non-uniform weights.

5 Conclusion

The purpose of this work was to evaluate the application of synchrophasing based on ESC as a tool for the reduction of noise at the fuselage skin in airplanes with DEP. To this end, a simulation tool was first developed to serve as a plant for the experiments.

The control system was tested in simulation scenarios considering two- and four-propeller configurations. For simplicity, only one side of the wingspan was considered. An array of 13 microphones arranged longitudinally along the fuselage was used as a set of observers. The cost function to be minimized by the controller was a weighted average of the RMS pressures at the microphones.

Extremum Seeking Control proved to be an effective tool to minimizing the SPL at selected observer locations. Its effectiveness, however, heavily depends on the selection of an appropriate cost function J_E in (18). Synchrophasing can only redirect the sound energy without causing a global reduction in the pressure levels at all locations. As a consequence, while certain directions perceive reduced SPL, other directions suffer an increase of the same. Synchrophasing is hence directional by nature. For a multi-fold reduction, allocating large weights to multiple microphones may or may not decrease the SPL at exactly those locations due to the spatial dependence of the phase difference which influences the interaction of the sound waves. This phenomenon was also seen in the two- and the four-propeller cases, where penalizing all the microphones did not necessarily lead to an overall reduction.

The synchrophase angles in the case of two-propellers converged to their minimizing arguments almost instantaneously and fluctuated very little during the steady state, as a result of the control action. The four-propeller case took roughly three seconds to converge and had a worse steady-state performance. There was a general tuning difficulty when more controlled variables were involved, and therefore more variables to be manipulated. The ESC output in this case was also more sensitive to variations in the tuning parameters and showed larger settling times.

Henceforth, future work includes using Sound Power Level instead of RMS pressures to define the cost function. A methodic definition of the weights of these functions based on certain goal is also an avenue to be explored. Furthermore, other control strategies beyond ESC are due to be studied.

References

[1] K. Ariyur and M. Krstic. *Real-Time Optimization by Extremum-Seeking Control*, chapter 1, pages 1–20. John Wiley & Sons, Ltd, 2003. ISBN 9780471669784. URL `https://onlinelibrary.wiley.com/doi/abs/10.1002/0471669784.ch1`.

[2] Bennett M. Brooks and F. B. Metzger. Acoustic test and analyses of three advanced turboprop models. Technical Report NASA CR-159667, NASA, Hamilton Standard, United Technologies Cor-

poration, Windsor Locks, Connecticut 06096, January 1980. URL https://api.semanticscholar.org/CorpusID:107244315.

[3] Jan Delfs. Grundlagen der aeroakustik (basics of aeroacoustics), ws 2022/2023, October 2022. URL https://www.dlr.de/en/as/downloads/dokumente/Notes_Basics_of_Aeroacoustics_Delfs.pdf. Lecture notes.

[4] Majid T. Fard, JiangBiao He, Hao Huang, and Yue Cao. Aircraft distributed electric propulsion technologies—a review. *IEEE Transactions on Transportation Electrification*, 8(4):4067–4090, 2022. doi: 10.1109/TTE.2022.3197332.

[5] Donald B. Hanson. Helicoidal surface theory for harmonic noise of propellers in the far field. *AIAA Journal*, 18(10):1213–1220, 1980. doi: 10.2514/3.50873. URL https://arc.aiaa.org/doi/abs/10.2514/3.50873.

[6] Donald B. Hanson and M.R. Fink. The importance of quadrupole sources in prediction of transonic tip speed propeller noise. *Journal of Sound and Vibration*, 62(1):19–38, 1979. URL https://doi.org/10.1016/0022-460X(79)90554-6.

[7] Harvey H. Hubbard. Aeroacoustics of flight vehicles: Theory and practice. volume 1: Noise sources. NASA Reference Publication 1258, Vol. 1, NASA Langley Research Center, 1991. URL https://ntrs.nasa.gov/citations/19920001380.

[8] Phillip Joseph, Chaitanya Paruchuri, Stephen Elliott, Mansi Bhardwaj, and Tze Pei Chong. Propeller tonal noise reductions through synchrophasing: Mechanisms and performance. *Journal of Sound and Vibration*, 610, 2025. URL https://doi.org/10.1016/j.jsv.2025.119110.

[9] Hyun Dae Kim, Aaron T. Perry, and Phillip J. Ansell. Progress in distributed electric propulsion vehicles and technologies. Technical report, NASA, 2020. URL https://api.semanticscholar.org/CorpusID:245985416.

[10] Andrés Lopez Pulzovan, Gaurav Bokil, and Thomas Geyer. An application of an extremum-seeking algorithm with improved gradient estimation for propeller noise control. In *30th International Congress on Sound and Vibration*, Amsterdam, NED, July 2024.

[11] Adrián Parra Lafuente, Andres Lopez Pulzovan, Rudy Cepeda-Gomez, and Thomas Geyer. Dynamic propeller noise reduction using synchrophasing control based on an extremum-seeking algorithm. In *AIAA Aviation Forum 2025*, 2025. URL `https://arc.aiaa.org/doi/10.2514/6.2025-3645`.

[12] D. Roy. Doppler frequency effects due to source, medium, and receiver motions of constant velocity. In *AIAA 8th Aeroacoustics Conference*, 1983. doi: 10.2514/6.1983-702. URL `https://arc.aiaa.org/doi/10.2514/6.1983-702`.

[13] Vítor Tumelero Valente. *Multiple Rotor Acoustic Control*. PhD thesis, Pennsylvania State University, 2024.

[14] Sascha Dominik Wolff. *Entwicklung von Fehlererkennungs-, Zustandsschätzungs-, Regelungs- und ganzzahligen Optimalsteuerungsmethoden für pulsierende, detonative Brennkammern anhand eines akustischen Ersatzsystems*. PhD thesis, Technische Universität Berlin, 2019.